DOI: 10.21062/mft.2026.020  http://www.journalmt.com

# 3D Printing – Dimensional Accuracy and Stability of PLA and PETG Prints Using the FDM Technology

Alexandr Fales (0009-0008-0055-611X)[1], Vít Černohlávek (0000-0001-6816-1124)[1], Marcin Suszynski (0000-0001-7926-0574)[2], Jan Štěrba (0000-0002-2676-3562)[1], Patrik Balcar (0009-0007-4924-5681) [1], Pavel Houška (0000-0003-4295-258X)[1]
[1]Faculty of Mechanical Engineering, J. E. Purkyne University in Usti nad Labem. Pasteurova 3334/7, 400 01 Usti nad Labem, Czech Republic. E-mail: alexandr.fales@ujep.cz, vit.cernohlavek@ujep.cz, jan.sterba@ujep.cz
[2]Faculty of Mechanical Engineering, Poznan University of Technology, marcin.suszynski@put.poznan.pl

**This study examines the influence of FDM printing parameters on replica parts for an educational robotics kit, targeting functional compatibility without post-processing. A VEX Robotics 2×12 Beam (228-2500-026) was used as the reference part. Reference dimensions were obtained as mean values from 10 original VEX IQ parts. Replicas were printed from PLA and PETG on Original Prusa MK4 printers using four infill patterns and six infill densities (15–70%). For each material–pattern–density combination, 10 parts were produced, resulting in 480 printed samples. Width, length, and height were measured with a Mitutoyo MiSTAR 555 CNC CMM in accordance with ISO 10360-2. Results are expressed as mean deviations from reference dimensions, standard deviations, and expanded uncertainty of the mean. Maximum deviations reached 0.062, 0.092, and 0.032 mm for PLA, and 0.046, 0.090, and 0.028 mm for PETG. The results provide guidance for selecting non-solid infill settings that reduce material use and printing time while maintaining dimensional compatibility.**

**Keywords:** 3D printing, FDM, Dimensional accuracy, PLA, PETG

## 1 Introduction

Educational robotics kits such as VEX GO and VEX IQ are widely used in schools for designing and validating robotic models. In such environments, parts are repeatedly assembled and disassembled and are exposed to typical handling loads. When components are missing, when a part variant is required, or when a design concept must be verified, Fused Deposition Modeling (FDM) offers an accessible method for manufacturing replacement parts directly at the point of use. For replicas to serve as functional substitutes for original components, dimensional conformity and compatibility without post-processing are essential, because post-processing is time-consuming and difficult to control in routine educational operation.

From a practical perspective, printing should be feasible for users without advanced process optimization and should avoid solid infill. Non-solid infill reduces filament consumption and printing time and may improve operational efficiency. However, the dimensional outcome of FDM printing depends on the process conditions and build strategy. In addition to material and machine settings, internal build pattern (infill topology and density) can influence the thermal history and residual stresses of the part and may therefore affect dimensional stability and repeatability. For this reason, the influence of infill settings on dimensional deviations should be experimentally verified for the intended application and constraints [1-3]. Triply periodic minimal surface (TPMS) architectures, such as gyroid-type infill, are frequently used in polymer additive manufacturing and represent a relevant alternative to conventional 2D patterns, motivating a controlled comparison of different infill topologies [4-6].

This study quantifies the dimensional accuracy and stability of FDM-printed replicas produced from two commonly used materials, PLA and PETG. A VEX Robotics structural component, the 2×12 Beam (228-2500-026), was selected as the reference element because it is frequently used in assemblies and its geometry enables repeatable metrological measurement of basic external dimensions. The reference dimensions were defined from measurements of original parts, and printed replicas were evaluated as deviations from these reference values. The part selection follows previous work reported in [7-9].

The objective of this study is to assess whether printing without post-processing can achieve dimensional conformity sufficient for practical compatibility, and to evaluate the influence of the material (PLA vs. PETG) and the infill parameters (pattern and density) on deviations of the main external dimensions width, length, and height. The results provide a basis for selecting infill settings that reduce material consumption and printing time while maintaining dimensional conformity required for educational use [10].

## 2 Materials and Methods

### 2.1 Reference part and reference dimensions

A structural element from the VEX Robotics construction system, the 2×12 Beam (228-2500-026), was selected as the reference part for the experimental evaluation of dimensional accuracy and stability. The part was chosen because it is commonly used in assemblies, is repeatedly assembled and disassembled, and its geometry enables stable and repeatable measurement of basic external dimensions.

For the quantitative comparison of original parts and 3D-printed replicas, three external reference dimensions were defined and evaluated: L (overall length) distance is between the two end faces of the beam (measured on the outer contour of the part), W (overall width) distance is between the two opposite outer side faces of the beam and H (overall profile height) distance is between the top and bottom outer surfaces of the part [11-13].

These dimensions were selected as the main indicators of overall dimensional conformity and potential shrinkage or deformation induced by the FDM process (influence of material and infill parameters). Hole pitch and hole diameters were not measured metrologically in this study, because the aim was not a geometric evaluation of the holes, but rather the verification of practical assembly usability under typical educational conditions.

Functional compatibility of the holes was assessed separately using a qualitative "PIN" test, i.e., a pass-through and fit check using the original connecting element referred to as PIN, which is used to join two or more parts. The following aspects were assessed: whether the PIN could be inserted into the hole, whether the assembled parts aligned properly without visible stress, and whether the joint retained the attached part in the required position during normal handling.

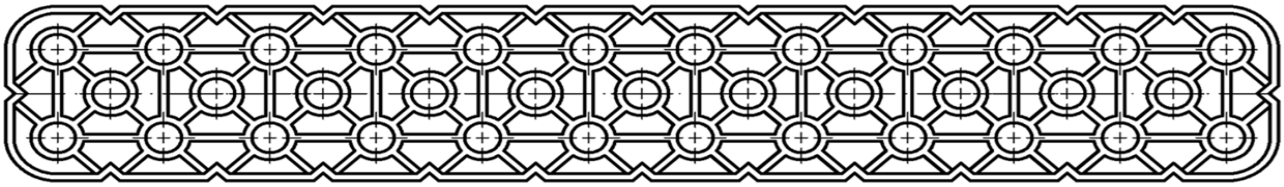

***Fig. 1*** *Reference part VEX Robotics 2×12 Beam (228-2500-026)*

### 2.2 Materials

Two commonly available materials for FDM 3D printing were used to manufacture the replicas: PLA and PETG. The selection reflects an educational context and the requirement to print without post-processing, considering availability, reliable printability, and sufficient mechanical performance for functional parts. PLA was selected due to its very good printability and low tendency to warp, making it suitable for rapid iterations in teaching. PETG was selected as a tougher alternative with higher resistance to service loading, while maintaining good printability when properly configured [14, 15].

In the experiment, Prusament filaments (Prusa Research) with a diameter of 1.75 mm were used. To clearly distinguish samples among different infill variants, the following colors were used (color served only for sample identification):

PLA (Prusament, 1 kg) – typical PLA material properties are listed in Tab. 1 and 3

- GRID: Prusament PLA Galaxy Silver
- GYROID: Prusament PLA Prusa Galaxy Black
- HONEYCOMB: Prusament PLA Galaxy Green
- TRIANGULAR: Prusament PLA Galaxy Red

***Tab. 1*** *Typical PLA material properties reported by the manufacturer*

| | **Typical value** | **Method/standard** |
|---|---|---|
| MFR [g/10 min](1) | 9–11 | ISO 1133 |
| MVR [cm³/10 min](1) | 8–10 | ISO 1133 |
| Density [g/cm³ ] | 1.24 | ISO 1183 |
| Moisture absorption after 24 hours [%](2) | 0.13 | Prusa Polymers |
| Moisture absorption after 7 days [%](2) | 0.19 | Prusa Polymers |
| Heat deflection temperature (0.45 MPa) [°C] | 55 | ISO 75 |
| Heat deflection temperature (1.80 MPa) [°C] | 55 | ISO 75 |
| Tensile strength of the filament [MPa] | 57 ± 1 | ISO 527 |
| Hardness – Shore D | 81 | Prusa Polymers |
| Interlayer adhesion [MPa] | 17 ± 3 | Prusa Polymers |
| *Note: The data were taken from the manufacturer's technical data sheet for PLA filament (Prusa Polymers), Version: 1.1, last update: 16-02-2022. (1) Test conditions: 2.16 kg; 210 °C. (2) Test conditions: 24 °C; relative humidity 22%.* | | |

PETG (Prusament, 1 kg) – typical PETG material properties are listed in Tab. 2 and 3

- GRID: Prusament PETG Terracotta Light
- GYROID: Prusament PETG Clear
- HONEYCOMB: Prusament PETG Jungle Green
- TRIANGULAR: Prusament PETG Lipstick Red

***Tab. 2*** *Typical PETG material properties reported by the manufacturer*

| | Typical value | Method/standard |
|---|---|---|
| MFR [g/10 min] | not reported | ISO 1133 |
| MVR [cm³/10 min] | not reported | ISO 1133 |
| Density [g/cm³ ] | 1.27 | ISO 1183 |
| Moisture absorption after 24 hours [%](1) | 0.07 | Prusa Polymers |
| Moisture absorption after 7 days [%](1) | 0.10 | Prusa Polymers |
| Heat deflection temperature (0.45 MPa) [°C] | 68 | ISO 75 |
| Heat deflection temperature (1.80 MPa) [°C] | 68 | ISO 75 |
| Tensile strength of the filament [MPa] | 46 ± 1 | ISO 527 |
| Hardness – Shore D | 74 | Prusa Polymers |
| Interlayer adhesion [MPa] | 18 ± 4 | Prusa Polymers |
| *Note: The data were taken from the manufacturer's technical data sheet for PETG filament (Prusa Polymers), Version: 1.1, last update: 16-02-2022. (1) Test conditions: 24 °C; relative humidity 22%.* | | |

***Tab. 3*** *Linear coefficient of thermal expansion (CTE) of PLA and PETG materials – literature value*

| Material | Value CTE [μm/(m·K)] | Method/standard |
|---|---|---|
| PLA | 68.0 | not specified |
| PETG | 68.4 | not specified |

Note: The CTE values were taken from the article PLA Filament Qualities 2023 (American Filament) [5]. The source does not specify the test method or the applicable standard.

The filaments were stored at FSI UJEP in the Destructive Testing Laboratory, where temperature and relative humidity were monitored. The filament was removed from the original plastic packaging only immediately before printing in the 3D printer. No filament drying was performed during the experiment, as the storage conditions and handling procedure were set to minimize the risk of moisture uptake.

### 2.3 Infill topology and infill density

From a large number of available infill patterns, four were selected for printing replicas intended for educational use of VEX IQ g2 parts (Grid, Triangular, Honeycomb, and Gyroid). These patterns provide a favorable balance between stiffness, strength, print time, and material consumption. Gyroid exhibits near-isotropic behavior and very good torsional and impact resistance, which is particularly advantageous for frames, brackets, and covers exposed to drops and multi-directional loading. Honeycomb and Triangular achieve high stiffness for plate-like and arm-type parts at the same mass and also support top surfaces well, helping parts retain their shape even under repeated assembly and disassembly. Grid is suitable for fast and easy-to-interpret prototypes of less critical components and, at the same time, serves a didactic purpose by illustrating the effect of "fiber" (extrusion path) orientation on resulting properties. All four patterns have smooth or predictable toolpaths, which reduces the risk of print defects for beginners; thanks to a more uniform stress distribution, they also better withstand screw and pin joints as well as impacts during student handling. The selected topologies also enable cost reduction, especially when lower infill densities are used.

Characteristics of the selected infills: Grid (rectilinear, 0/90°) – Geometry and toolpath: two orthogonal families of lines, alternating 0/90° between layers; many crossings and start/stop events. Printing: very fast and simple to plan, but the higher number of interruptions can reduce bonding between adjacent extruded lines. Mechanical properties: good stiffness and strength along the extrusion directions (X/Y); pronounced anisotropy (weaker diagonal, shear, and torsion); higher stress concentrations at nodes; lower impact and fatigue resistance compared to the other patterns. Suitable for: rapid prototypes and parts loaded mainly along the extrusion directions; less suitable for diagonal loading. Triangular – Geometry and toolpath: triangular cells; directions typically rotate by 60° between layers; relatively continuous trajectories. Printing: medium print time; fewer interruptions than Grid; good support of top surfaces. Mechanical properties: high specific stiffness and strength in-plane; better shear stiffness and bending stability of plates than Grid; good energy absorption; mild anisotropy out of plane. Suitable for:

thin-walled plates and covers with in-plane bending; parts requiring higher stiffness at low mass. Honeycomb – Geometry and toolpath: closed hexagonal cells; smooth loops with minimal start/stop. Printing: longer than Grid but very consistent; excellent support of top surfaces. Mechanical properties: high stiffness and strength in compression/bending of plate-like parts; good shear stiffness and decent impact resistance; in very thin walls, local buckling may occur under high loads. Suitable for: lightweight and stiff panels, cover infills, and parts requiring uniform surface support. Gyroid (TPMS – triply periodic minimal surface) – Geometry and toolpath: a 3D continuous periodic surface without sharp edges; in the slicer, smooth and nearly uninterrupted paths. Printing: smooth, with few joints; for 2D patterns, the actual "effective" density at the same nominal infill density may differ. Mechanical properties: close to 3D isotropy; excellent shear and torsional stiffness; high impact and fatigue resistance due to the absence of pronounced stress concentrators; very good behavior in compression and energy absorption. Suitable for: multi-directionally loaded and torsion-loaded parts, energy-absorbing elements, and parts requiring repeatability and cohesion [16–18].

For experimental verification of dimensional accuracy and in subsequent research on the mechanical properties of printed replicas of VEX IQ g2 parts, a set of relative infill densities of 15, 25, 40, 50, 60, and 70% was selected across the Grid, Triangular, Honeycomb, and Gyroid patterns. This range covers the region in which, according to scaling laws for cellular materials, stiffness and strength increase nonlinearly and failure mechanisms change: at 15–25%, lightweight and time-efficient configurations with expected lower stiffness and higher energy dissipation capability are tested; medium densities of 40–50% represent a practical optimum of specific stiffness/strength with respect to mass and print time for educational use; higher densities of 60–70% map the region of diminishing returns and verify strength limits, where interlayer bonding and local stress concentrations begin to dominate. Solid infill (100%) was not included because, in FDM, it leads to a disproportionate increase in mass and print time for a relatively small marginal gain in stiffness/strength; it also increases thermal load and the risk of internal defects and warping. From the perspective of ratio metrics (e.g., $E/\varrho$, $\sigma/\varrho$) and cost effectiveness, 100% infill therefore typically does not provide a meaningful improvement over 60–70%. Note: in PrusaSlicer, Grid is often the default for very low infill values.

As part of print preparation, the parameters used in PrusaSlicer were also recorded for individual parts. For example, for the 2×12 Beam (228-2500-026) VEX part, the following settings were used: PrusaSlicer 2.9.4, PLA material, Gyroid infill pattern, 15% infill density.

### 2.4 Printers and printing conditions

All printed replicas were manufactured at the Faculty of Mechanical Engineering, J. E. Purkyne University in Usti nad Labem FSI UJEP, using FDM on an Original Prusa MK4 3D printer. Print data preparation was performed in PrusaSlicer 2.9.4. A standard 0.4 mm brass nozzle was used. The VEX Robotics 2×12 Beam (228-2500-026) was printed flat on the build plate to improve adhesion, ensure a more consistent layer structure, and enable printing without supports. An example of the PrusaSlicer settings for one parameter combination is shown in Fig. 2. Supports were not used and no post-processing was performed. The layer height was set to 0.15 mm (Structural profile) and the number of perimeters to 2. Print speeds and cooling settings were not further optimized and were kept at the default PrusaSlicer profile settings for the Original Prusa MK4 for the given material (PLA or PETG). The infill pattern Grid, Triangular, Honeycomb, Gyroid and infill density 15%, 25%, 40%, 50%, 60%, and 70% were used as variable parameters in the experiment. Material-specific temperatures and the build plate type were set as follows: PLA—nozzle 210–215 °C, build plate 50–60 °C, smooth PEI sheet without additional adhesion; PETG—nozzle 240–250 °C, build plate 85–90 °C, satin sheet, with 3DLAC spray used for adhesion. An overview of all printing parameters is provided in Tab. 4. The number of printed replicas for each parameter combination and the print scheduling/organization are described in Chapter 2.5. Examples of the printed replicas made from PLA and PETG are shown in Figs. 3 and 4. The photographic documentation is included as evidence of evaluation in the as-printed condition, without any post-processing, i.e., without sanding, edge chamfering, or other modifications. It enables visual verification that the dimensional deviations and scatter measured on the CMM directly reflect the outcome of the FDM process and are not affected by subsequent interventions that would be time-consuming and difficult to standardize in typical school environment.

### 2.5 Impact of the build plate and filament quality on print success in a school environment

Successful 3D printing primarily depends on the adhesion of the first layer to the build plate. If adhesion is insufficient, the print may detach during the printing process, leading to print failure and rendering the part unusable. In a school environment, where time and technical support are often limited, first-layer stability is a key prerequisite for reliable production. The selected Original Prusa printer uses removable magnetic build plates with different surface

finishes (smooth PEI, satin, or textured), and the choice of a suitable plate depends on the material used. For PLA, a smooth PEI sheet was used; if necessary, adhesion can be improved using an adhesive aid (e.g., 3DLAC spray). PETG, by contrast, exhibits high adhesion; therefore, it is recommended to use a satin or textured sheet and apply a separation layer to reduce the risk of damaging the sheet surface. Before each print, the build plate was degreased with isopropyl alcohol (IPA), which removes grease residues and contributes to consistent first-layer adhesion. Details on filament storage and handling prior to printing are provided in Chapter 2.2, Materials. Recommendations regarding the choice of build plate surface, IPA cleaning, and the use of a separation layer for PETG are consistent with commonly cited operating procedures for Original Prusa printers [19-21].

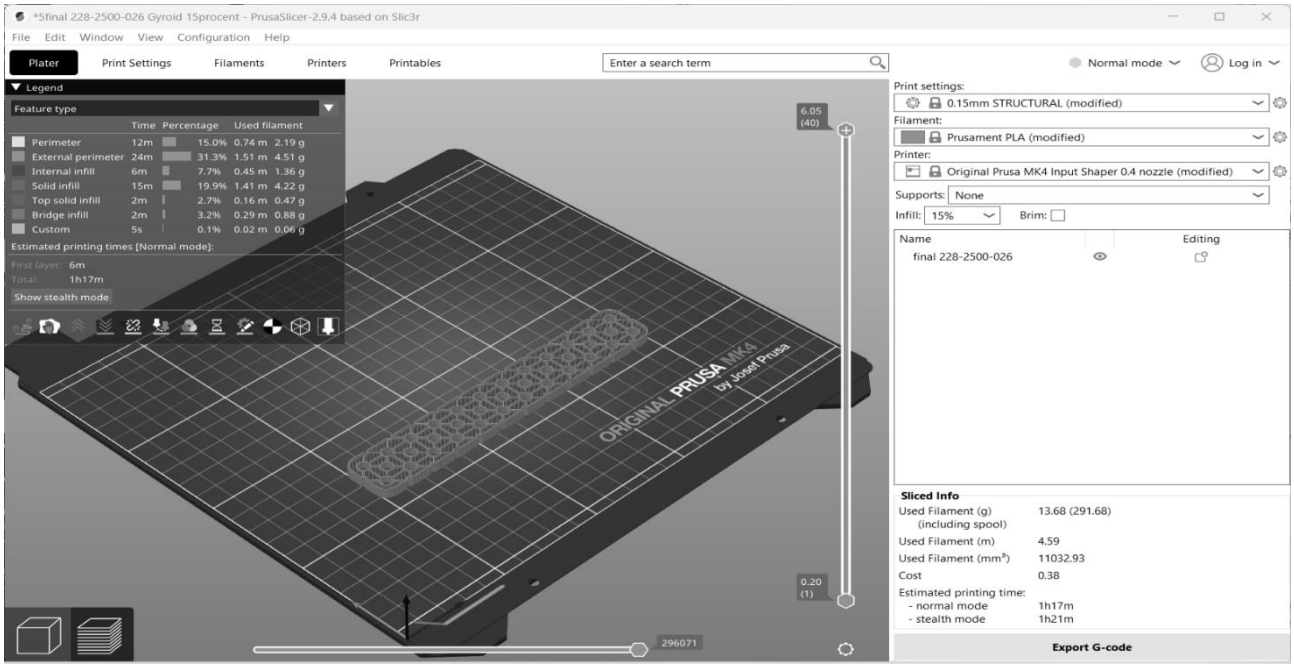


***Fig. 2*** *Settings for PrusaSlicer 2.9.4 — 2x12 Beam (228-2500-026) VEX — PLA material — Gyroid 15%*

***Tab. 4*** *Printing and Material-specific parameters*

| Parameter | Setting / value |
|---|---|
| 3D printer | Original Prusa MK4 |
| Printing location | FSI UJEP |
| Slicer | PrusaSlicer 2.9.4 |
| Profile | 0.15 mm – Structural |
| Technology | FDM |
| Nozzle diameter | 0.4 mm |
| Nozzle material | Brass (standard) |
| Layer height | 0.15 mm |
| Number of perimeters | 2 |
| Part orientation | Flat on the build plate |
| Supports | Not used |
| Post-processing | Not performed |
| Print speeds | Default PrusaSlicer profile for Original Prusa MK4 (no modifications) |
| Cooling (fan) | Default PrusaSlicer profile for the given material (no modifications) |
| Infill density (variable) | 15%, 25%, 40%, 50%, 60%, 70% |
| Infill pattern (variable) | Grid, Triangular, Honeycomb, Gyroid |
| Replicas per combination | 10 parts (material × pattern × density) |
| Total printed replicas | 480 parts (240 PLA + 240 PETG) |
| Original reference parts | 10 parts |

| Material-specific parameters | | | | |
|---|---|---|---|---|
| **Material** | **Nozzle temperature** | **Build plate temperature** | **Build plate** | **Build plate adhesion** |
| PLA | 210–215 °C | 50–60 °C | Smooth PEI sheet | None |
| PETG | 240–250 °C | 85–90 °C | Satin sheet | 3DLAC (spray) |

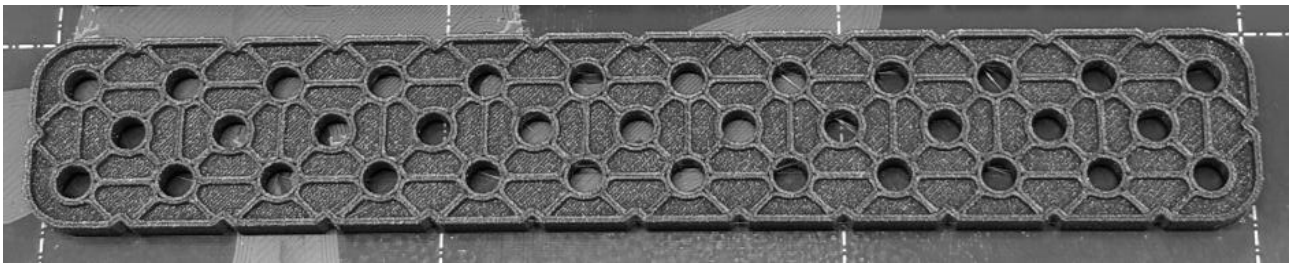

***Fig. 3*** *Print of a replica of the VEX Robotics 2x12 Beam (228-2500-026) VEX part from PLA material*

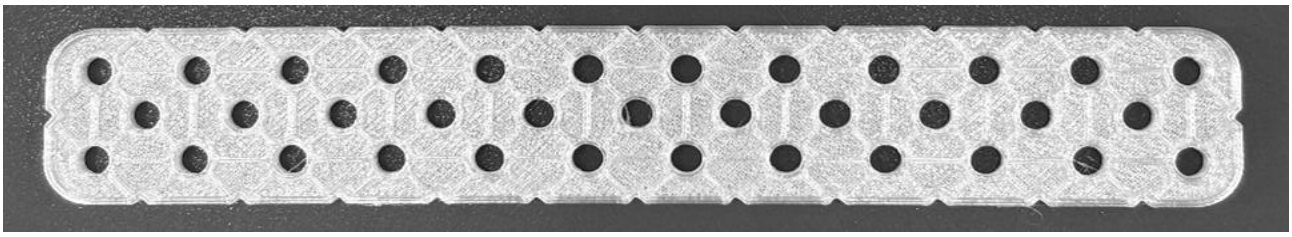

***Fig. 4*** *Print of a replica of the VEX Robotics 2x12 Beam (228-2500-026) VEX part from PETG material*

### 2.6 Experimental design and sample size

The experiment was designed as a full-factorial study with three factors: material (PLA and PETG), infill pattern (Grid, Triangular, Honeycomb, and Gyroid), and infill density (15%, 25%, 40%, 50%, 60%, and 70%). In total, 48 combinations (2 × 4 × 6) were produced. For each combination, n = 10 replicates were printed, resulting in 480 printed replicas in total (240 PLA and 240 PETG). For comparison with the original part, 10 original reference parts were also included. The number of replicates (10) was selected with regard to the inherent variability of the FDM process and the need to obtain representative estimates of both the mean and the variance for subsequent statistical comparisons. The experimental factors were material, infill pattern, and infill density. All other printing parameters were kept constant as specified in Section 2.4 and Tab. 4. Printing was organized in blocks by material: first, a series of PLA replicas was printed, followed by a series of PETG replicas. Within each material block, the pattern × density combinations were produced in random order to reduce the effect of process time drift over the course of the print series.

For PETG, occasional material transfer from the nozzle to the print surface was observed. A print was rejected if the local surface protrusion in the Z direction reached ≥ 1.0 mm and could affect the measured properties. This criterion was verified visually for rapid identification of suspected deposits and, as a check, using an a Mitutoyo ABSOLUTE ABS AOS digital caliper with a resolution of 0.001 mm. Each measurement was performed three times, and the highest measured value was used for the acceptance decision. Rejected parts were replaced by reprinting to ensure that 10 acceptable replicates were available for each parameter combination.

### 2.7 Dimensional measurement (CMM) and measurement conditions

The aim of the dimensional measurement was to determine the dimensional deviations of the printed replicas of the VEX Robotics 2×12 Beam (228-2500-026) part relative to the reference dimensions of the original part, and to evaluate dimensional conformity and manufacturing repeatability when printing without any post-processing. The measurements were carried out on a Mitutoyo MiSTAR 555 coordinate measuring machine (Code No. 357-305), illustrated in Fig. 5. The evaluated dataset followed the experimental design described in Section 2.5 and comprised 480 printed replicas and 10 original reference parts.

Measurement procedure: sample preparation and labeling; visual inspection and a qualitative PIN test, CMM setup and definition of the measured dimensions W, L, and H, measurement execution and data recording, statistical processing ($\bar{x}$, s) and evaluation of deviations relative to the reference; the expanded uncertainty of the mean was determined in accordance with GUM.

Dimensional measurements were performed on a coordinate measuring machine (CMM) Mitutoyo MiSTAR 555 (Code No. 357-305) with a measuring range of 500 × 500 × 400 mm (X × Y × Z). The CMM accuracy is specified according to ISO 10360-2 and, due to the integrated temperature compensation technology, varies with ambient temperature. The maximum permissible error of length measurement is expressed as:

- Standard conditions (18–22 °C): $E_{0,MPE} = 2.2 + 3L/1000$ μm
- Extended conditions (10–30 °C): $E_{0,MPE} = 2.9 + 4.5L/1000$ μm

- Maximum range (10–40 °C): $E_{0,MPE} = 3.8 + 8L/1000$ μm

Where:

L…The measured length in millimetres. The native system resolution is 0.0001 mm.

The measurements were performed fully automatically in CNC mode using a PH10MQ touch-trigger probe equipped with a 1 mm stylus ball. The measured dimensions were length L, width W, and height H. Each dimension was measured using a three-point strategy (both edges and the center), and the measurement system reported the average value. For the purposes of this experiment, the output resolution - i.e., the increment/rounding of the reported values – was set to 0.001 mm, which increased measurement speed while maintaining the usability of the results. Given that prints made from PLA and PETG were measured, this level of precision is more than sufficient for the intended purpose. Each part was measured twice, and the average of the two measurements was used for evaluation. The measured values were read from the measurement system display and manually recorded in a Microsoft Excel spreadsheet. Recording and readback verification were performed with two persons present; the second person served as an ongoing check of correct reading and data entry.

### 2.8 Measurement conditions


***Fig. 5*** *Professional measuring system Mitutoyo Mistar 555*

Measurements were performed under the following laboratory conditions:

- Temperature: 20.8–20.9 °C
- Air pressure: 997.9–998.4 hPa
- Relative humidity: 34.9–35.1%

For evaluation, the mean value of the measured dimensions was used.

### 2.9 Measurement uncertainty

Measurement uncertainty was evaluated as a combination of a Type A component derived from repeatability and Type B components derived from the CMM specification and the resolution/rounding of the reported values, in accordance with the GUM methodology [6]. The expanded uncertainty $U$ was determined for a coverage factor $k = 2$, corresponding approximately to a 95% coverage level [22].

The following assumptions were used: measuring machine: Mitutoyo MiSTAR 555; accuracy specified according to ISO 10360-2 by the relation $E_{0,MPE}$ [7], measurement conditions: approximately 20.8–20.9 °C, i.e., within the standard range of 18–22 °C, reported values rounded to 0.001 mm, each part measured twice, with the average value used for evaluation.

The uncertainty of the mean was determined in accordance with [6] as follows:

$$u_A = \frac{s_L}{\sqrt{n}} \tag{1}$$

$$E_{0,MPE} = 2.2 + \frac{3 \cdot L}{1000}\ [\mu m] \tag{2}$$

$$u_{CMM} = \frac{E_{0,MPE}}{\sqrt{3}} \tag{3}$$

$$u_{res} = \frac{0.0005}{\sqrt{3}} \tag{4}$$

$$u_c = \sqrt{u_A^2 + u_{CMM}^2 + u_{res}^2} \tag{5}$$

$$U = k \cdot u_c, k = 2 \tag{6}$$

As an example, for the reference group (original part, $n = 10$) and dimension $L$, the following values were obtained: $\bar{L} = 152.010$ mm and $s_L = 0.001498$ mm. The Type A component was therefore:

$$u_A = \frac{s_L}{\sqrt{n}} = \frac{0{,}001498}{\sqrt{10}} = 0{,}000474 \text{ mm} \tag{7}$$

For $L \approx 152$ mm, the CMM contribution under standard conditions according to ISO 10360-2 [7] was:

$$E_{0,MPE} = 2.2 + \frac{3 \cdot L}{1000} = 2.2 + \frac{3 \cdot 152}{1000} = 2.656\ \mu m \tag{8}$$

$$u_{CMM} = \frac{E_{0,MPE}}{\sqrt{3}} = \frac{2.656}{\sqrt{3}} = 1.533\ \mu m = 0.001533\ \text{mm} \quad (9)$$

The rounding component was:

$$u_{res} = \frac{0.0005}{\sqrt{3}} = 0.000289\ \text{mm} \quad (10)$$

The combined standard uncertainty and expanded uncertainty were then:

$$u_c = \sqrt{u_A^2 + u_{res}^2 + u_{CMM}^2} = \sqrt{0.000474^2 + 0.001533^2 + 0.000289^2} = 0.00163\ \text{mm} \quad (11)$$

$$U = k \cdot u_c = 2 \cdot 0.00163 = 0.00326\ \text{mm} \quad (12)$$

Thus, for this example, the result for dimension $L$ was $\bar{L} = 152.010$ mm with $U(k = 2) \approx \pm 0.00326$ mm.

The same procedure was applied to dimensions $W$ and $H$ and to all evaluated groups. The resulting expanded uncertainties are reported in Tabs. 5 and 6. Across groups, the values of $U$ were similar because the uncertainty was dominated mainly by the Type B components, whereas the Type A contribution was smaller for $n = 10$.

## 3 Results

The results are summarized in Tabs. 5 and 6. Explanations of the reported values are provided in a consolidated note below the tables.

***Tab. 5/1*** *PLA Material - variability of dimensions among parts and expanded uncertainty of the estimated mean (k = 2; GUM)*

| Group | Dimension | $\bar{x}$[mm] | s [mm] | U [mm] (k=2) |
|---|---|---|---|---|
| original (full) | W | 25.0960 | 0.00172 | 0.00290 |
| | L | 152.0100 | 0.00149 | 0.00325 |
| | H | 6.0100 | 0.00169 | 0.00284 |
| 15% infill – Triangular | W | 25.0440 | 0.00171 | 0.00318 |
| | L | 151.9420 | 0.00229 | 0.00369 |
| | H | 6.0380 | 0.00327 | 0.00440 |
| 15% infill – Honeycomb | W | 25.0340 | 0.00141 | 0.00301 |
| | L | 151.9180 | 0.00143 | 0.00303 |
| | H | 6.0290 | 0.00117 | 0.00295 |
| 15% infill – Gyroid | W | 25.0510 | 0.00186 | 0.00331 |
| | L | 151.9590 | 0.00197 | 0.00350 |
| | H | 6.0280 | 0.00184 | 0.00334 |
| 15% infill – Grid | W | 25.0530 | 0.00203 | 0.00341 |
| | L | 151.9740 | 0.00189 | 0.00346 |
| | H | 6.0230 | 0.00138 | 0.00303 |
| 25% infill – Triangular | W | 25.0600 | 0.00206 | 0.00342 |
| | L | 151.9340 | 0.00215 | 0.00366 |
| | H | 6.0320 | 0.00235 | 0.00367 |
| 25% infill – Honeycomb | W | 25.0410 | 0.00225 | 0.00353 |
| | L | 151.9490 | 0.00227 | 0.00373 |
| | H | 6.0280 | 0.00169 | 0.00327 |
| 25% infill – Gyroid | W | 25.0480 | 0.00159 | 0.00310 |
| | L | 151.9500 | 0.00286 | 0.00422 |
| | H | 6.0270 | 0.00166 | 0.00326 |
| 25% infill – Grid | W | 25.0700 | 0.00136 | 0.00299 |
| | L | 151.9260 | 0.00132 | 0.00296 |
| | H | 6.0280 | 0.00155 | 0.00317 |
| 40% infill – Triangular | W | 25.0510 | 0.00135 | 0.00299 |
| | L | 151.9250 | 0.00140 | 0.00303 |
| | H | 6.0350 | 0.00132 | 0.00298 |
| 40% infill – Honeycomb | W | 25.0420 | 0.00218 | 0.00348 |
| | L | 151.9360 | 0.00211 | 0.00362 |
| | H | 6.0420 | 0.00147 | 0.00310 |
| 40% infill – Gyroid | W | 25.0420 | 0.00107 | 0.00288 |
| | L | 151.9360 | 0.00159 | 0.00321 |
| | H | 6.0350 | 0.00175 | 0.00329 |

***Tab. 5/2*** *PLA Material - variability of dimensions among parts and expanded uncertainty of the estimated mean (k = 2; GUM)*

| Group | Dimension | x̄[mm] | s [mm] | U [mm] (k=2) |
|---|---|---|---|---|
| 40% infill – Grid | W | 25.0690 | 0.00092 | 0.00284 |
| | L | 151.9300 | 0.00127 | 0.00295 |
| | H | 6.0390 | 0.00111 | 0.00291 |
| 50% infill – Triangular | W | 25.0440 | 0.00199 | 0.00340 |
| | L | 151.9350 | 0.00275 | 0.00413 |
| | H | 6.0370 | 0.00267 | 0.00398 |
| 50% infill – Honeycomb | W | 25.0580 | 0.00194 | 0.00336 |
| | L | 151.9460 | 0.00192 | 0.00339 |
| | H | 6.0360 | 0.00181 | 0.00333 |
| 50% infill – Gyroid | W | 25.0590 | 0.00175 | 0.00325 |
| | L | 151.9500 | 0.00327 | 0.00483 |
| | H | 6.0340 | 0.00135 | 0.00304 |
| 50% infill – Grid | W | 25.0740 | 0.00139 | 0.00300 |
| | L | 151.9400 | 0.00229 | 0.00374 |
| | H | 6.0260 | 0.00150 | 0.00311 |
| 60% infill – Triangular | W | 25.0520 | 0.00097 | 0.00295 |
| | L | 151.9340 | 0.00183 | 0.00337 |
| | H | 6.0420 | 0.00179 | 0.00332 |
| 60% infill – Honeycomb | W | 25.0500 | 0.00112 | 0.00298 |
| | L | 151.9460 | 0.00159 | 0.00317 |
| | H | 6.0370 | 0.00112 | 0.00299 |
| 60% infill – Gyroid | W | 25.0510 | 0.00120 | 0.00300 |
| | L | 151.9540 | 0.00183 | 0.00337 |
| | H | 6.0320 | 0.00141 | 0.00307 |
| 60% infill – Grid | W | 25.0790 | 0.00129 | 0.00303 |
| | L | 151.9210 | 0.00136 | 0.00300 |
| | H | 6.0310 | 0.00081 | 0.00292 |
| 70% infill – Triangular | W | 25.0520 | 0.00107 | 0.00296 |
| | L | 151.9400 | 0.00181 | 0.00335 |
| | H | 6.0380 | 0.00178 | 0.00332 |
| 70% infill – Honeycomb | W | 25.0460 | 0.00162 | 0.00343 |
| | L | 151.9500 | 0.00111 | 0.00298 |
| | H | 6.0340 | 0.00110 | 0.00295 |
| 70% infill – Gyroid | W | 25.0520 | 0.00140 | 0.00305 |
| | L | 151.9520 | 0.00108 | 0.00297 |
| | H | 6.0280 | 0.00144 | 0.00306 |
| 70% infill – Grid | W | 25.0780 | 0.00177 | 0.00329 |
| | L | 151.9320 | 0.00179 | 0.00332 |
| | H | 6.0290 | 0.00162 | 0.00315 |

***Tab. 6/1*** *PETG Material - variability of dimensions among parts and expanded uncertainty of the estimated mean (k = 2; GUM)*

| Group | Dimension | x̄ [mm] | s [mm] | U [mm] (k=2) |
|---|---|---|---|---|
| original (full) | W | 25.0960 | 0.00172 | 0.00290 |
| | L | 152.0100 | 0.00149 | 0.00325 |
| | H | 6.0100 | 0.00169 | 0.00284 |
| 15% infill – Triangular | W | 25.0510 | 0.00119 | 0.00299 |
| | L | 151.9340 | 0.00114 | 0.00298 |
| | H | 6.0330 | 0.00202 | 0.00342 |
| 15% infill – Honeycomb | W | 25.0580 | 0.00165 | 0.00316 |
| | L | 151.9320 | 0.00132 | 0.00302 |
| | H | 6.0290 | 0.00163 | 0.00315 |
| 15% infill – Gyroid | W | 25.0700 | 0.00131 | 0.00302 |
| | L | 151.9310 | 0.00173 | 0.00327 |
| | H | 6.0280 | 0.00162 | 0.00315 |
| 15% infill – Grid | W | 25.0560 | 0.00183 | 0.00334 |
| | L | 151.9230 | 0.00157 | 0.00312 |
| | H | 6.0190 | 0.00107 | 0.00296 |

***Tab. 6/2*** *PETG Material - variability of dimensions among parts and expanded uncertainty of the estimated mean (k = 2; GUM)*

| Group | Dimension | $\bar{x}$ [mm] | s [mm] | U [mm] (k=2) |
|---|---|---|---|---|
| 25% infill – Triangular | W | 25.0540 | 0.00139 | 0.00303 |
| | L | 151.9350 | 0.00172 | 0.00324 |
| | H | 6.0260 | 0.00166 | 0.00321 |
| 25% infill – Honeycomb | W | 25.0660 | 0.00141 | 0.00304 |
| | L | 151.9250 | 0.00148 | 0.00312 |
| | H | 6.0290 | 0.00162 | 0.00315 |
| 25% infill – Gyroid | W | 25.0690 | 0.00142 | 0.00304 |
| | L | 151.9260 | 0.00205 | 0.00350 |
| | H | 6.0270 | 0.00204 | 0.00349 |
| 25% infill – Grid | W | 25.0560 | 0.00183 | 0.00334 |
| | L | 151.9300 | 0.00148 | 0.00312 |
| | H | 6.0220 | 0.00126 | 0.00301 |
| 40% infill – Triangular | W | 25.0500 | 0.00111 | 0.00298 |
| | L | 151.9360 | 0.00128 | 0.00301 |
| | H | 6.0330 | 0.00192 | 0.00339 |
| 40% infill – Honeycomb | W | 25.0680 | 0.00108 | 0.00297 |
| | L | 151.9250 | 0.00184 | 0.00337 |
| | H | 6.0280 | 0.00224 | 0.00363 |
| 40% infill – Gyroid | W | 25.0700 | 0.00132 | 0.00302 |
| | L | 151.9240 | 0.00171 | 0.00327 |
| | H | 6.0300 | 0.00183 | 0.00332 |
| 40% infill – Grid | W | 25.0600 | 0.00144 | 0.00306 |
| | L | 151.9220 | 0.00116 | 0.00300 |
| | H | 6.0270 | 0.00157 | 0.00312 |
| 50% infill – Triangular | W | 25.0500 | 0.00111 | 0.00298 |
| | L | 151.9340 | 0.00095 | 0.00296 |
| | H | 6.0290 | 0.00203 | 0.00342 |
| 50% infill – Honeycomb | W | 25.0700 | 0.00089 | 0.00294 |
| | L | 151.9220 | 0.00134 | 0.00303 |
| | H | 6.0290 | 0.00168 | 0.00322 |
| 50% infill – Gyroid | W | 25.0640 | 0.00112 | 0.00298 |
| | L | 151.9320 | 0.00167 | 0.00321 |
| | H | 6.0300 | 0.00205 | 0.00344 |
| 50% infill – Grid | W | 25.0620 | 0.00141 | 0.00305 |
| | L | 151.9290 | 0.00144 | 0.00306 |
| | H | 6.0320 | 0.00162 | 0.00315 |
| 60% infill – Triangular | W | 25.0530 | 0.00094 | 0.00295 |
| | L | 151.9320 | 0.00160 | 0.00314 |
| | H | 6.0270 | 0.00203 | 0.00342 |
| 60% infill – Honeycomb | W | 25.0700 | 0.00156 | 0.00311 |
| | L | 151.9310 | 0.00119 | 0.00299 |
| | H | 6.0380 | 0.00216 | 0.00355 |
| 60% infill – Gyroid | W | 25.0610 | 0.00111 | 0.00298 |
| | L | 151.9330 | 0.00131 | 0.00302 |
| | H | 6.0280 | 0.00167 | 0.00322 |
| 60% infill – Grid | W | 25.0670 | 0.00129 | 0.00301 |
| | L | 151.9200 | 0.00143 | 0.00306 |
| | H | 6.0290 | 0.00162 | 0.00315 |
| 70% infill – Triangular | W | 25.0560 | 0.00073 | 0.00293 |
| | L | 151.9300 | 0.00160 | 0.00314 |
| | H | 6.0350 | 0.00203 | 0.00342 |
| 70% infill – Honeycomb | W | 25.0710 | 0.00102 | 0.00296 |
| | L | 151.9280 | 0.00194 | 0.00305 |
| | H | 6.0290 | 0.00165 | 0.00321 |
| 70% infill – Gyroid | W | 25.0540 | 0.00077 | 0.00293 |
| | L | 151.9270 | 0.00194 | 0.00340 |
| | H | 6.0300 | 0.00143 | 0.00308 |
| 70% infill – Grid | W | 25.0720 | 0.00143 | 0.00305 |
| | L | 151.9240 | 0.00173 | 0.00327 |
| | H | 6.0240 | 0.00164 | 0.00316 |

Note on the tables: The tables report the mean values $\bar{x}$, the sample standard deviations $s$ representing part-to-part variability within each group, and the expanded uncertainties of the mean $U$ for $k = 2$, determined in accordance with the GUM and including Type A and Type B components. In each group, $n = 10$ parts were evaluated; for each part, the average of two measurements was used.

The mean values $\bar{x}$ describe the location of the dimension within the individual groups, whereas $s$ expresses the within-group (part-to-part) variability. Across all groups, $s$ is on the order of thousandths of a millimetre (0.0007 to 0.0033 mm), without an obvious trend across infill densities and infill types.

The expanded uncertainty of the mean $U$ is very similar across groups, on the order of 0.0028 - 0.0048 mm. This is due to the dominance of Type B components: rounding of the readout to 0.001 mm ($u_{\mathrm{res}} = 0.0005/\sqrt{3} = 0.00289$ mm) and the CMM contribution from the specification $E_{(0.\mathrm{MPE})}$, which depends on the measured length. In contrast, the Type A component, calculated as $u_A = s/\sqrt{n}$, is on the order of $\approx 0.0002$–0.0010 mm for $n = 10$, and therefore has a smaller effect on the resulting $U$. The tables thus provide two distinct pieces of information: 1) the within-group part variability $s$ and 2) the uncertainty of the estimated group mean $U$.

## 4 Discussion

### 4.1 Key findings: dimensional accuracy, repeatability, and material differences

Dimensional measurement of replicas of the VEX Robotics 2×12 Beam (228-2500-026) part on a coordinate measuring machine (CMM) demonstrated high manufacturing repeatability: the sample standard deviations $s$ of the individual dimensions across configurations are on the order of thousandths of a millimetre—approximately 0.00081 to 0.00327 mm for PLA and 0.00073 to 0.00224 mm for PETG—indicating a stable printing and measurement process. At the same time, the replicas exhibit a consistent systematic offset (bias) relative to the reference dimensions of the original part, i.e., primarily a shift in the mean $\bar{x}$ between groups rather than increased random part-to-part variability. It should be emphasized that the resolution of the reported values was set to 0.001 mm for the purposes of the experiment, and the evaluation was based on a three-point measurement strategy with averaging (two repetitions per part); the expanded uncertainty of the mean $U$ (for $k = 2$) is therefore relatively similar across groups and is largely determined by Type B components (in particular the contribution of resolution/rounding and the length-dependent contribution of the measurement system), whereas the Type A component $u_A = s/\sqrt{n}$ is smaller for $n = 10$ and has a limited impact on the resulting $U$. This is consistent with the $U$ values reported in the tables: for PLA, $U$ ranges approximately from 0.00284 to 0.00483 mm, whereas for PETG $U$ is more stable, approximately 0.00293 to 0.00363 mm. Even with this setting, the results clearly indicate stable and predictable process behaviour.

For the PLA dataset (15–70%), the trend is unambiguous:

- $W$ is smaller than the original in all cases ($\Delta W_{\mathrm{ref}} = -0.0620$ to $-0.0170$ mm),
- $L$ is smaller than the original in all cases ($\Delta L_{\mathrm{ref}} = -0.0920$ to $-0.0360$ mm),
- $H$ is larger than the original in all cases ($\Delta H_{\mathrm{ref}} = +0.0130$ to$+0.0320$ mm).

For the PETG dataset (15–70%), the bias relative to the original is likewise consistent:

- $W$ is smaller than the original in all cases ($\Delta W_{\mathrm{ref}} = -0.024$ to $-0.046$ mm),
- $L$ is smaller than the original in all cases ($\Delta L_{\mathrm{ref}} = -0.076$ to $-0.090$ mm),
- $H$ is larger than the original in all cases ($\Delta H_{\mathrm{ref}} = +0.014$ to$+0.028$ mm).

From a practical perspective, this combination of low scatter $s$ and stable bias means that printing is highly repeatable, but the resulting part is systematically shifted relative to the original. This is advantageous in practice: a stable offset can be deliberately compensated through process settings or scaling, whereas high random variability would be more problematic for educational use. For functional compatibility within a construction-kit system, it is also important to recognize that even deviations on the order of hundredths of a millimetre can affect clearance and friction in an assembly (especially at interfaces with other parts). For this reason, it is advisable to complement the dimensional evaluation with a simple functional verification (see the recommendations in Section 4.3).

### 4.2 Balance of Stiffness, Strength, Print Time, and Material Use

The observed direction of deviations (negative bias in XY, positive bias in Z) is consistent with typical FDM behavior and can be explained by a combination of mechanisms: Thermal shrinkage during cooling (material and process dependent). After extrusion, the deposited filament cools and undergoes volumetric changes. In the layer plane (XY), this often manifests as a slight "pull-in" of dimensions, especially along longer features (here, L). Differences in bias

magnitude between configurations can be understood as the result of different thermal histories (cooling rate, local heat accumulation) and thus different shrinkage levels. Build-plate adhesion and constrained deformation in early layers. The first layers are partially constrained by adhesion to the build plate, which affects how internal stresses relax during cooling and can amplify differences between XY behavior and Z behavior. Residual stresses and their relaxation. Temperature gradients during printing generate internal stresses that can relax during or after printing, producing small but systematic changes in shape and measured dimensions. The low SD indicates these effects are repeatable rather than random. Z-axis specifics (positive H bias). A positive height deviation can result from cumulative layer-wise effects (actual vs. nominal layer thickness), extrusion flow settings, and first-layer behavior (Z-offset and first-layer compression). Even small per-layer deviations can accumulate into a consistent H bias.

Why do infill pattern and density have only a small effect on external dimensions? External dimensions are primarily governed by the outer perimeters (shells) and their toolpath placement. Infill is internal; its influence on the exterior is mostly indirect—through thermal balance, support of top layers, and changes in internal stress distribution. When perimeter settings and top/bottom layers are stable, changes in infill typically affect mechanical performance and print time more than they alter external dimensions. This matches the present results: the bias direction (W and L smaller, H larger) remains consistent across infill patterns and densities.

From the perspective of practical use in schools, the key point is that the results indicate predictable behavior: the parts do not vary randomly, but exhibit a repeatable offset that can be taken into account during manufacturing.

### 4.3 Practical recommendations for educational use

For typical educational use (fast availability, adequate robustness, minimal tuning), a mid-range infill density of 40–50% is recommended as a pragmatic compromise. This choice generally balances: print time and material consumption (substantially lower than 60–70%), sufficient internal support for stable top-layer formation, mechanical robustness for handling and repeated assembly in class.

From a dimensional-accuracy perspective: If the goal is the best possible match to the original, it is more effective to address it primarily via systematic-bias compensation (e.g., fine XY scaling, flow tuning, and Z-offset/first-layer control) than by searching for an "optimal" infill pattern. The data indicate the bias is stable and therefore compensable. For functional compatibility in a construction system, dimensional analysis should be complemented by a simple functional fit test (e.g., a pin test), because deviations on the order of hundredths of a millimeter can influence clearance and friction. In practice: choose infill mainly for stiffness/strength and print time, and address dimensional matching through targeted process tuning and compensation.

### 4.4 Limitations and future work

The results should be interpreted in light of several limitations. First, the study focused on only one part geometry, namely the VEX IQ Robotics 2×12 Beam (228-2500-026). Different geometries, such as parts with larger flat areas, thinner walls, or different hole and rib configurations, may exhibit different deformation modes and different sensitivity to infill structure. Second, the experiment was conducted using a single printer and specific process settings, which limits the direct transferability of the results to other machines, printer conditions, and slicing profiles. The systematic bias strongly depends on the specific machine, its calibration, mechanical condition, slicer profile, and environmental conditions. Transferability to other printers requires verification. Therefore, strong claims regarding the superiority of one material over the other should be avoided unless both materials are compared over the same infill range. Short-term stability only. The study does not address long-term aging, moisture effects, thermal cycling, creep, or stress relaxation over time. These factors may affect dimensions and functional performance in real educational use. No direct link to mechanical testing. The optimal compromise recommendation is based primarily on dimensional accuracy, repeatability, and practical considerations (print time, material use), not on directly measured strength or stiffness. For this reason, further research will follow, focusing on destructive experimental tests (e.g., bending/tension/compression depending on the intended application) printed replicas as a function of material, infill pattern, and infill density, and to recommend print parameters for specific use cases in robotics education.

## 5 Economics of Printing (basic calculation)

### 5.1 Print time and material usage (PETG, 50%)

Tab. 7 summarizes print time and filament mass for PETG at 50% infill using four infill patterns. These two variables are the main inputs for a basic per-part cost estimate and they also determine printer capacity – how many parts can be produced within a given time window.

***Tab. 7*** *Values from PrusaSlicer – print time and mass*

| Material | Infill pattern | Infill [%] | Print time [h:min] | Time [min] | Mass [g] |
|---|---|---|---|---|---|
| PETG | Gyroid | 50 | 1:42 | 102 | 16.22 |
| PETG | Grid | 50 | 1:31 | 91 | 16.30 |
| PETG | Honeycomb | 50 | 1:48 | 108 | 16.95 |
| PETG | Triangular | 50 | 1:31 | 91 | 16.40 |

In terms of time, the fastest options are Grid and Triangular, at 91 min, while Honeycomb is the slowest 108 min. The maximum difference is 17 min per part, which accumulates noticeably when printing multiple parts and directly affects available printer capacity in a school environment.

### 5.2 Basic cost calculation (material + electricity)

The calculation is intentionally limited to direct variable costs – filament and electricity – and does not include printer depreciation, print preparation, supervision, or post-processing. The goal is to compare variants and obtain an approximate per-part cost suitable for educational use.

Input values:

- Filament price (PLA and PETG): 1 kg spool 32.99 €/kg, i.e. 0.033 €/g
- Electricity price: 0.18 €/kWh
- Approximate average power draw of the Original Prusa MK4: for PLA, approx. 80 W; for PETG, approx. 80–100 W (slightly higher due to higher build plate temperature)

For broader applicability, costs can be rescaled linearly with filament price (€/kg) and electricity price (€/kWh).

Equations used:

- Material cost per part:

$$C_{\text{mat}} = \left(\frac{m}{1000}\right) \cdot C_{\text{kg}} \text{(equivalently: } C_{\text{mat}} = m \cdot 0.033\text{)} \tag{13}$$

- Electricity cost per part (approximate):

$$C_{\text{el}} = \left(\frac{P}{1000}\right) \cdot t \cdot C_{\text{kWh}} \tag{14}$$

Where:
P…The power in W,
t…The time in hours,
$C_{\text{kWh}}$ = 0.18 €/kWh.

- Time difference: difference in minutes between variants.
- Results – PETG 50% (material + electricity)

Material cost (exact, from mass):

- PETG Gyroid 50% (16.22 g): $16.22 \times 0.033 = 0.535$ €/part
- PETG Grid 50% (16.30 g): $16.30 \times 0.033 = 0.538$ €/part
- PETG Honeycomb 50% (16.95 g): $16.95 \times 0.033 = 0.559$ €/part
- PETG Triangular 50% (16.40 g): $16.40 \times 0.033 = 0.541$ €/part

Electricity cost (approximate; PETG 80–100 W):

- Gyroid 1:42 (1.70 h): $(0.08–0.10)$ kW × 1.70 h × 0.18 €/kWh = 0.024–0.031 €/part
- Grid 1:31 (1.52 h): 0.022–0.027 €/part
- Honeycomb 1:48 (1.80 h): 0.026–0.032 €/part
- Triangular 1:31 (1.52 h): 0.022–0.027 €/part

Total cost (material + electricity; interval):

- PETG Gyroid 50%: 0.559–0.566 €/part
- PETG Grid 50%: 0.560–0.565 €/part
- PETG Honeycomb 50%: 0.585–0.591 €/part
- PETG Triangular 50%: 0.563–0.568 €/part

### 5.3 Check example – PLA calculator output

For PLA with 15% Gyroid infill, the check example was based on values obtained from the Prusa online print cost calculator [10]: print time approximately 1 h 16 min, filament mass 13.69 g, filament price 32.99 €/kg, material cost 0.45 €, and electricity cost 0.018 €. The reported material cost is consistent with the calculation based on filament mass and unit price: 13.69 × 0.033 = 0.45 €. Electricity costs 0.02 € in this example; compared to the material cost, it is a minor item.

Summary (interpretation for school environment): The basic calculation indicates that, at a filament price of 32.99 €/kg, a PETG part (50% infill) costs approximately 0.559–0.591 € per part including

approximate electricity. Differences between infill patterns are small in terms of material on the order of cents, while print time is more operationally important: up to 17 min per part, which directly affects printer capacity in a school setting. The reported values represent minimum direct costs excluding failed prints; for real-world operation, a waste factor for failed prints and supports is often applied, e.g. 1.2×.

## 6 Conclusion

The aim of this study was to experimentally verify whether FDM printing on an Original Prusa MK4 can produce replicas of the VEX Robotics 2×12 Beam (228-2500-026) from PLA and PETG with dimensional agreement and repeatability sufficient for functional compatibility without any post-processing, and to assess the influence of infill topology (Grid, Triangular, Honeycomb, Gyroid) and infill density (15–70%) on the external dimensions W, L, and H. Reference dimensions were defined as the arithmetic mean of measurements of ten original parts, and the printed replicas were evaluated as deviations from these reference values. Dimensional measurements were performed on a Mitutoyo MiSTAR 555 coordinate measuring machine (CMM) in CNC mode with temperature compensation according to ISO 10360-2; results were reported using means, sample standard deviations, and the expanded uncertainty of the mean (k = 2) evaluated in accordance with GUM.

From the standpoint of manufacturing repeatability, all parameter combinations exhibited low part-to-part variability: the sample standard deviations of the dimensions, $s$, across groups were on the order of thousandths of a millimetre (PLA approximately 0.00081 to 0.00327 mm, PETG approximately 0.00073 to 0.00224 mm) with no apparent monotonic trend with respect to infill topology or density. The expanded uncertainty of the mean, $U$ (for $k = 2$), was relatively stable across groups and ranged from 0.00284 to 0.00483 mm for PLA and 0.00293 to 0.00363 mm for PETG. The dominant contribution arose from Type B components (in particular the rounding/resolution of the reported output to 0.001 mm and the length-dependent contribution of the measurement system), whereas the Type A component $\left(u_A = s/\sqrt{n}\right)$ was typically smaller for $n = 10$ and had a limited effect on the resulting $U$. The results therefore confirm a stable and reproducible printing and measurement process within the chosen experimental setup.

At the same time, a consistent systematic offset (bias) relative to the original part was observed for both materials: in the XY plane, dimensions $W$ and $L$ were smaller than the reference values in all cases, while along the Z axis the height $H$ was larger than the reference. For PLA, the maximum observed deviations were 0.062 mm (W), 0.092 mm (L), and 0.032 mm (H); for PETG they were 0.046 mm (W), 0.090 mm (L), and 0.028 mm (H). Practically, the key point is that this is a repeatable offset with low scatter, which is advantageous in an educational setting: a stable bias can be deliberately compensated through process adjustments (e.g., XY scaling, fine-tuning the extrusion flow rate, and checking the first-layer Z-offset), whereas high random variability would be more problematic for functional compatibility.

Within the scope of this study, the influence of infill topology and density on the external dimensions appeared secondary compared to material/process effects and to perimeter and layer settings, which primarily define the external geometry. Therefore, it is reasonable to select infill mainly based on printing time, material consumption, and the expected mechanical robustness, while addressing dimensional agreement through targeted compensation of the systematic offset and simple functional verification. Hole compatibility was assessed qualitatively using a PIN test, which is a suitable complement to dimensional evaluation in the school environment, since even deviations on the order of hundredths of a millimetre may affect clearance and friction in assemblies.

From an economic perspective (based on slicer-reported printing times and material usage), for PETG at 50% infill the part mass ranged from 16.22 to 16.95 g and the printing time from 91 to 108 min depending on the infill topology. A difference of up to 17 min per part is operationally more significant than the differences in material usage, because it directly limits printer throughput. For educational use, mid-range infill densities of 40–50% represent a practical compromise, typically reducing material consumption and printing time while maintaining stable and predictable dimensional behaviour.

Future work will focus on follow-up destructive mechanical testing (e.g., bending and tensile tests) as a function of material, infill topology, and infill density, and on verifying the long-term dimensional and mechanical stability of printed parts under school operating conditions (ageing, humidity, thermal cycling, creep), including the effects of storage and exposure to heat and UV radiation.

## Acknowledgement

***This article was supported by the SGS grant of J. E. Purkyne University in Usti nad Labem, project No. UJEP-SGS-2025-48-001-1, and by the project DigiLab SMART III – Ustecký kraj, registration number CZ.02.01.02/00/22_009/0004316, implemented within the OP JAK programme.***

## References


[1] FALES, A., ČERNOHLÁVEK, V., SUSZYNSKI, M., ŠTĚRBA, J., ZDRÁHAL, T., NOCAR, D. (2025). Experimental Measurement and Testing of 3D Printed Parts in Terms of the Material Used. In: *Manufacturing Technology*, pp. 174 – 184. DOI 10.21062/mft.2025.016

[2] CHACÓN, J.M., CAMINERO, M.A., GARCÍA-PLAZA, E., NÚÑEZ, P.J. (2017). Additive manufacturing of PLA parts by fused deposition modeling: Effect of process parameters on mechanical properties. In: *Materials & Design*, Vol. 124, pp. 143 – 157. DOI 10.1016/j.matdes.2017.03.065

[3] ZIEMIAN, C.W., ZIEMIAN, S., HAILE, K. (2012). Characterization of stiffness and strength of FDM manufactured parts. In: *Rapid Prototyping Journal*, Vol. 18, No. 2, pp. 131 – 143. DOI 10.1108/13552541211212196

[4] ABUEIDDA, D.W., BAKIR, M., AL-RUB, R.K.A., BERGSTRÖM, J.S., SOBH, N.A., JASIUK, I. (2017). Mechanical properties of 3D printed polymeric cellular materials with triply periodic minimal surface architectures. In: *Materials & Design*, pp. 255 – 267. DOI 10.1016/j.matdes.2017.03.018

[5] FALES A. (2023). Educational Robotics. In: *Proceedings of the International Conference Experimental and Computational Methods in Engineering*, pp. 169 – 172. Usti nad Labem. ISBN 978-80-7561-411-7

[6] (2025). PLA Filament Qualities. In: *American Filament*: https://americanfilament.us/blogs/3d-printing-guide/pla-filament-properties

[7] FALES, A., ČERNOHLÁVEK, V., ŠTĚRBA, J., DIAN, M., SUSZYNSKI, M. (2025). Innovative Approaches to Material Selection and Testing in Additive. In: *Materials*, Vol. 18, pp 144 – 168. DOI 10.3390/ma18010144

[8] (2008). JCGM 100:2008: Evaluation of measurement data – Guide to the expression of uncertainty in measurement (GUM). In: *Joint Committee for Guides in Metrology*

[9] (2009). ISO 10360-2:2009: *Geometrical product specifications (GPS) – Acceptance and reverification tests for coordinate measuring machines* (CMM) – Part 2: CMMs used for measuring linear dimensions. Geneva: International Organization for Standardization

[10] (2025). Guide materials. In: *Prusa Research*. https://help.prusa3d.com/cs/category/pruvodce-materialy_220

[11] ČERNOHLÁVEK, V., ŠTĚRBA, J., SVOBODA, M., ZDRÁHAL, T., SUSZYNSKI, M., CHALUPA, M., KROBOT, Z. Verification of the safety of storing a pair of pressure vessels. In: *Manufacturing Technology*, Vol. 21, No. 6, pp:762 – 773. DOI 10.21062/mft.2021.097

[12] HORNE, R., HAUSMAN, K.K. (2023). *3D Printing For Dummies. 3rd ed. Hoboken,* NJ: John Wiley & Sons. ISBN 978-1394169474

[13] (2025). 3D Printing Price Calculator. In: *Prusa Research*. https://blog.prusa3d.com/3d-printing-price-calculator_38905/

[14] PONIKELSKÝ, J.; CHALUPA, M.; ČERNOHLÁVEK, V.; ŠTĚRBA, J. (2024). Force and Pressure Dependent Asymmetric Workspace Research of a Collaborative Robot and Human. In: *Symmetry*, Vol. 16, pp. 131. DOI 10.3390/sym16010131

[15] JIN, F., LU, W., AN, X., ZHU, H., WANG, J. (2024). Mechanical Properties and Compression Performance of 3D Printed HIPS Polymer Lattice Structure. In: *Manufacturing Technology*, Vol. 24, No. 3, pp 378 – 392. DOI 10.21062/mft.2024.054.

[16] SUSZYŃSKI, M.; WIŚNIEWSKI, M.; WOJCIECHOWICZ, K.; TRACZYŃSKI, M.; BUTLEWSKI, M.; ČERNOHLÁVEK, V.; TALAR, R. (2025) Study of Positioning Accuracy Parameters in Selected Configurations of a Modular Industrial Robot – Part 1. In: *Sensors*, Vol. 25, pp. 108. DOI 10.3390/s25010108

[17] KLIMENDA, F., KAMPO, J., HEJMA, P. (2016) Vibration Measurement of Conveyor Rollers. In: *Procedia Engineering*, Vol. 136, pp. 198 – 203. ISSN 1877-7058, DOI 10.1016/j.proeng.2016.01.197.

[18] BECHNÝ, V., MATUŠ, M., JOCH, R., DRBÚL, M., CZÁN, A., ŠAJGALÍK, M., NOVÝ, F. (2024). Influence of the Orientation of Parts Produced by Additive Manufacturing on Mechanical Properties. In: *Manufacturing Technology*, Vol. 24, No. 1, pp 2 – 8. DOI 10.21062/mft.2024.021.

[19] SAPIETA, M., ŠULKA, P., SVOBODA, M. (2018) Localization of delamination in composite test specimens. In: *MATEC Web of Conferences*, pp. 157. DOI 10.1051/matecconf/201815701015

[20] CHALUPA, V., STANEK, M., VANEK, J., STRNAD, J., OVSIK, M. (2023). Design of Dual-Head 3D Printer. In: *Manufacturing Technology*, Vol. 23, No. 2. pp 177 – 185. DOI 10.21062/mft.2023.032.

[21] SVOBODA, M., SOUKUP, J., PETRENKO, A. (2015) Use of MBD Programs in Solving General Unbalance Simple Mechanical System. In: *Applied Mechanics and Materials*, Vol. 732, pp. 275 – 282. Trans Tech Publications, Switzerland. DOI: 10.4028/www.scientific.net/AMM.732.275

[22] SAPIETA, M., ŠULKA, P., SVOBODA, M. (2018). Using a numerical model to verification of thermoelastic analysis of flat specimen. In: *Manufacturing Technology*, Vol. 18, No. 3, pp 482 – 486. ISSN: 1213-2489, DOI: 10.21062/ujep/125.2018/a/1213-2489/MT/18/3/482